Pergamon

Int. J. Multiphase Flow Vol. 22, No. 3, pp. 431–452, 1996

0301-9322/96 $15.00 + 0.00

0301-9322(95)00086-0

DROP FORMATION MECHANISMS AND SIZE DISTRIBUTIONS FOR SPRAY PLATE NOZZLES†

G. E. MCCREERY and C. M. STOOTS

Lockheed Idaho Technologies Company, Idaho National Engineering Laboratory, Idaho Falls, ID, U.S.A.

(Received 25 April 1995, in revised form 11 December 1995)

Abstract—This article describes the results of an experimental investigation of drop formation mechanisms and drop diameter distributions for spray plate nozzles. Spray plate nozzles are comprised of a distribution nozzle which projects a high velocity jet of water concentric on a plate. The resultant water film flows radially outward on the plate and breaks into drops after the liquid detaches from the plate and flows outward as a sheet. The drop size distribution is determined by a balance between shear forces with air and flow instabilities and turbulence in the liquid sheet flow, which tend to fracture the liquid sheet and drops, and surface tension forces, which tend to hold the liquid sheet and drops together. Experimental results include short duration photographs of nozzle jet flow, liquid film flow, and of water drop formation. Drop diameter distributions were obtained with a phase Doppler particle analyzer (PDPA). The variations of drop mean diameter, volumetric mean and Sauter mean diameters as functions of pressure, distribution nozzle-to-plate distance, and plate diameter are quantified. Copyright © 1996 Elsevier Science Ltd.

Key Words: drop, drop size distribution, liquid jet, liquid sheet, spray nozzle

INTRODUCTION

An experimental investigation of drop formation mechanisms, drop diameter distributions, and spray distributions for spray plate nozzles was conducted. This generic type of nozzle is commonly used for center pivot agricultural irrigation and for fire protection and is available in a variety of designs from a number of manufacturers. The nozzle is comprised of a distribution nozzle which projects a high velocity (turbulent) jet of water concentric on a plate (see figure 1). The resultant water film flows radially outward on the plate, detaches from the plate as a liquid fan sheet, and then breaks into drops. The drop size distribution is determined by a balance between shear forces with air and flow instabilities and turbulence in the liquid sheet flow, which tend to fracture the liquid sheet and drops, and surface tension forces, which tend to hold the sheet and drops together.

The objective of the research was to develop fundamental knowledge of drop formation in spray nozzles and obtain data which will help to optimize spray nozzle designs. In order to reduce water consumption and, therefore, electric power consumption, it is desirable to improve the uniformity of irrigation spray patterns and to decrease the rate of water evaporation. Water evaporation and soil erosion are determined to a large extent by water drop diameter distributions of a sprays. Small drops (smaller than approximately one millimeter in diameter (Kincaid & Longley 1989)) evaporate more readily than larger drops and are transported by wind more easily than larger drops since the ratio of drop surface area divided by volume (proportional to the inverse of radius) is larger for smaller drops. Both the heat transfer rate per unit mass and the wind force per unit mass are in turn approximately proportional to radius to the minus one power. Soil erosion, on the other hand, is caused primarily by drops larger than approximately two millimeters in diameter (Kincaid 1993). Larger drops travel further and have more impact energy than smaller drops. In addition to causing erosion, larger drops are to a large extent responsible for the problem of "soil sealing", whereby the pores in the soil surface are mechanically and chemically sealed, and the flow of water into the soil is impeded. The optimum drop diameter distribution for most irrigation sprays is therefore one with the majority of diameters lying between approximately 1 and 2 mm.

†Work supported by the United States Department of Energy under DOE Idaho Operations Office contract DE-AC07-941D13223.

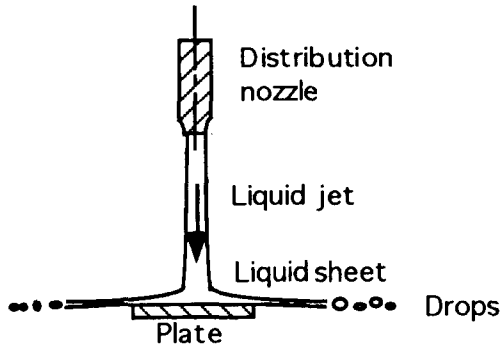

Figure 1. Spray plate nozzle.

This article concentrates on drop formation phenomena and drop diameter distributions. An equally important aspect of spray nozzle design is the distribution of drops over the surface or volume sprayed. This aspect was investigated, but is beyond the scope of the present article.

The fluid dynamics of liquid jets impinging on surfaces has been studied by a number of investigators. The primary interest of the majority of these studies has been the high heat transfer rates available to surfaces from impinging liquid jets. Examples of research on impinging jets which are of use for the present research include the characterization of liquid flow and boundary layer formation on a plate by Stevens & Webb (1992) and Buyevich & Ustinov (1994). Investigations of the heat transfer of impinging liquid jets include those by Liu *et al.* (1993), Elison & Webb (1994), and others. The flow structure in turbulent liquid jets was investigated by Hoyt & Taylor (1979), Mansour & Chigier (1994) and others. Liquid jets impinging on a flat surface may splatter and expel drops from the liquid surface upstream of a hydraulic jump as discussed by Bhunia & Lienhard V (1994a, 1994b). According to the authors, the amount of splattering is governed by the level of surface disturbances present on the surface of the liquid jet (spray plate nozzles are designed to avoid splattering, since splattering reduces the kinetic energy of the drops and spray radius).

The instability of a thin moving free liquid sheet, such as is encountered after the liquid sheet detaches from the plate, was studied analytically by Squire (1953). He concluded that a moving sheet is unstable and that, for liquid sheets moving in gas, waves grow with a predominant wavelength,

$$\lambda = \frac{4\pi\sigma}{\rho_G U^2} \qquad [1]$$

where ρ_G is gas density, σ is surface tension, and U is sheet velocity. Taylor (1960) performed experiments to investigate radially spreading liquid sheets formed by two colliding water jets in air. He determined that the analytical results of Squire (1953) give reasonable results under the assumption that sheet velocity equals jet velocity. Huang (1970) performed experiments on colliding jets and investigated the breakup mechanisms of the liquid sheets. He identified two breakup regimes plus a transition regime as a function of jet Weber number ($We_j = \rho_L U_j^2/\sigma$, where U_j is jet velocity). In the first regime, drops are formed through successive merging of liquid beads along the nearly circular periphery of the sheet. The second regime is characterized by the axisymmetric waves described above (all of the data presented in this paper falls within the second regime). A semi-empirical equation was formulated by the author to predict the breakup radius of the sheet. For the first regime (We_j less than approximately 800), the breakup radius was determined by a balance between surface tension and inertial forces, and was found to increase proportional to We_j to the first power. For the second regime (We_j greater than approximately 1,000), the motion of the sheet was related to a vibrating membrane with steadily decreasing thickness, and the breakup radius was found to decrease with We_j to approximately the $-1/3$ power.

Reviews of drop formation mechanisms are given in Clift *et al.* (1978), Lefebvre (1989), and by Kolev (1993). Models for the formation of drops from the breakup of liquid sheets are given by Dombrowski & Jones (1963), who described the breakup as due to growing sinusoidal disturbances

which break into cylindrical ligaments, and then into drops. According to the authors, the process is governed by surface tension, aerodynamic and liquid viscous forces. They obtain a volume average drop equal to 1.88 times the ligament diameter, similar to the breakup of a cylindrical jet first described by Raleigh (1878). Chin *et al.* (1991) employed a maximum entropy formalism to investigate the drop diameter distribution from the breakup of a cylindrical liquid jet. Van der Geld & Vermeer (1994) described the breakup of unstable ligaments into primary and satellite drops as following a maximum entropy formalism. Spielbauer & Aidun (1994) measured the radial thinning of liquid sheets and describe the localized breakup as due to perforations in the sheet. Yarin (1993) examined the breakup of a perforated sheet using percolation theory and derived a size distribution. Experimental studies of drop size distributions for agricultural spray nozzles include those by Solomon *et al.* (1985), Solomon *et al.* (1991), and Kinkaid (1993). These studies characterized a wide variety of commercially available spray nozzles under a wide range of flow conditions rather than investigated the design parameters of one type of nozzle, as does the present study. Hawkes *et al.* (1992) photographed the breakup of water jets from an impact type nozzle and investigated the effects of wind perpendicular to the jet. The main effects of wind were an enhanced breakup of larger drops and a narrowing of spray width.

In this article experimental methods and experimental results are described. The experimental apparatus and the conduct of experiments are first described. The results include short duration (4 μs) photographs of nozzle jet flow, liquid film flow on the spray plate, and of water drop formation, and drop diameter distribution data obtained with a phase Doppler particle analyzer (PDPA). Data uncertainty is discussed, phenomena observed, and drop diameter distributions and other data are presented.

EXPERIMENT APPARATUS

The experiment apparatus is shown schematically in figure 2. The apparatus consists of a "spray booth" within which the nozzle is positioned. The spray exiting the spray booth is confined to a narrow (3–4 cm) width by adjustable shutters. The exit spray flows through a measurement region and is then captured by a chevron baffle box and flows as a liquid film into the drain trough. Both the spray booth and baffle box are placed within the drain trough. The water flow path is from a building water spigot through a pressure regulator, then through a phase separator tank (to remove any air bubbles from solution), into a distribution plenum (5.01 cm i.d.) and then downward through a 1.90 cm i.d. pipe to the nozzle. The plumbing is designed to insure that flow delivered to the nozzle is steady, well developed (turbulent), and free from periodic vortex shedding and flow oscillations. Line pressure upstream of the distribution plenum was measured with a

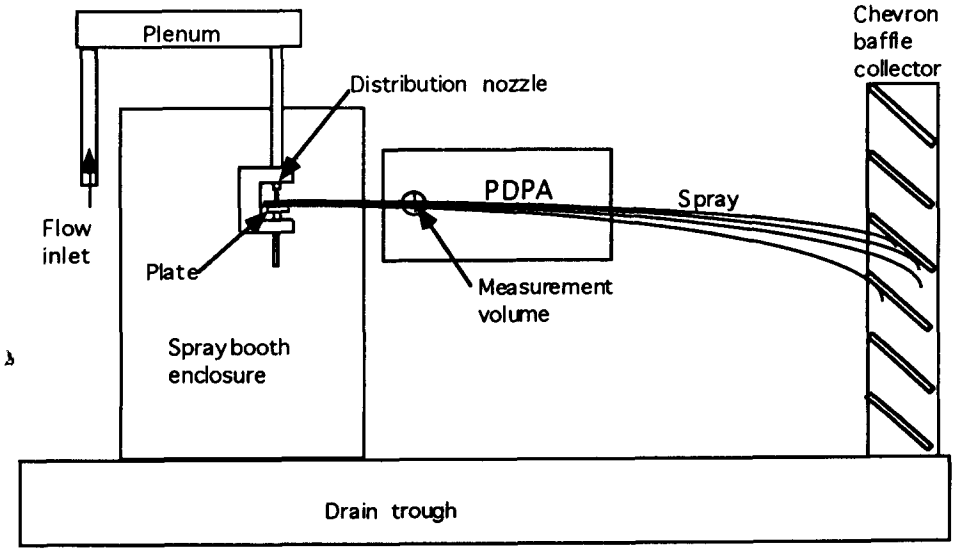

Figure 2. Experiment apparatus showing plumbing, adjustable nozzle, and PDPA optics.

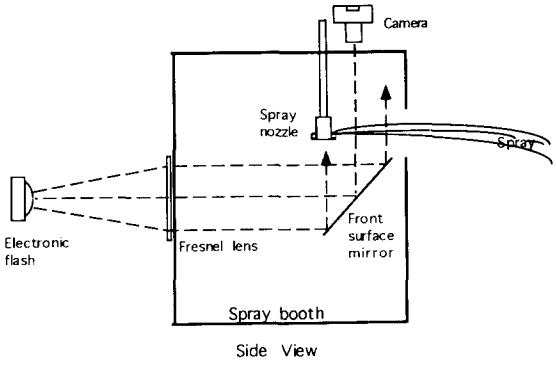

Figure 3. Bright field illumination.

pressure gauge and used to set the flow conditions. Flow rates for each delivery nozzle were calibrated as a function of pressure. In addition to pressure and flow rate, water temperature was measured and recorded.

Commercially available spray plate nozzles (Nelson Irrigation) were used for photography. An adjustable spray plate nozzle was used for the experiments. The nozzle was constructed to provide replaceable flat spray plates of various diameters (0.89, 1.27, 1.90, 2.54, 3.18, 3.81 and 5.08 cm diameters), adjustable nozzle to plate spacing of from 0.0 to 10.8 cm, and replaceable delivery nozzles. Commercially available (Nelson Irrigation) delivery nozzles with 3.18 and 2.29 mm inside diameters were primarily used. The nozzles have a simple conical into straight cylindrical bore, with a chamfered exit. Water temperatures for the data reported in this article were $12 \pm 0.5^{\circ}C$, with temperature variations of less than the measurement uncertainty of $\pm 0.2^{\circ}C$ during each experiment.

Photographs were taken using a Pentax 35 mm single-lens reflex camera with 100 mm macroscopic lens and a Sunpak 611 electronic flash, and with a 10.2×12.7 cm view camera using an EG&G electronic strobe which was modified to provide a single flash capability with a flash duration of 4 μs. The Sunpak flash had a minimum duration of approximately 56 μs, which was adequate for capturing many details, but permitted a movement of approximately 0.1 cm of water drop and jet surface features for a typical jet velocity of approximately 18 m/s at a delivery pressure of 172 kPa gauge, as calculated by Bernoulli's equation. The short duration 4 μs strobe permitted photographs of water drops with no apparent blurring due to motion.

A variety of lighting techniques were employed for the photographs. In general, bright field illumination (figure 3) was the most successful technique for photographing drops, and dark field illumination (figure 4) was most successful for photographing the jet and liquid fan sheet before breakup into drops. Kodak T_{max} 100 film was used for the majority of 35 mm photographs, and Kodak T_{max} 400 and Polaroid Type 55 (positive–negative) film was used for the large format photographs.

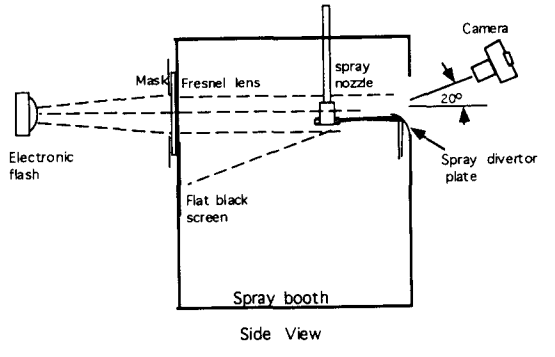

Figure 4. Dark field illumination.

Drop diameter distributions were obtained using an Aerometrics PDPA which uses the light scattered by spherical particles (drops, bubbles, or solid particles) to obtain simultaneous size and velocity measurements (Bachalo *et al.* 1990). Drop velocity distributions were also measured, but the measurements are not discussed in the present article. Drops passing through the intersection of two laser beams scatter light which produces a far field interference fringe pattern. The spacing between the projected fringes is inversely proportional to the drop diameter but is also dependent on the light wavelength, beam intersection angle, drop refractive index, and the location of the receiver. The temporal frequency of the measured signal is proportional to the particle velocity component in the plane of the beams and orthogonal to the bisector of beams. The overall size range which may be detected by the PDPA is from 0.5 to 3,000 μm. However, the maximum range of diameters measurable at one setting is a factor of 35. The majority of diameter measurements obtained in these experiments were with a range of from 85.7 to 3,000 μm, which included the large majority of drops produced by sprays under study (measurements were also taken to characterize the size distribution for drops less than 85.7 μm in diameter, and the few drops larger than 3,000 μm may be measured from the photographs). The PDPA was operated in the backscattered light mode using a 300 mW Omnichrome argon–ion laser. Signals were monitored using a Hewlett–Packard digital storage oscilloscope to insure that accurate alignment and adequate signal strength were maintained throughout the duration of experimentation.

Drop diameter mean (d_{10}), volume mean (d_{30}), and Sauter mean (d_{32}), the volume divided by surface area mean (used primarily for heat transfer calculations), were calculated by the PDPA software. In general, 10,000 individual drop measurements were obtained to produce each drop diameter distribution. The large number of measurements was necessary because the range of drop diameters was large, and because relatively few large diameter (2,000–3,000 μm) drops were produced. The few large drops, however, have a disproportionately large influence on the calculated volume and Sauter mean drop sizes.

Drop size distributions were obtained over ranges of pressure, plate diameter, and nozzle to plate spacing for two nozzle sizes (3.18 and 2.29 mm i.d.). The nozzle to plate spacings of 2.22 and 4.76 cm correspond to commercially available nozzles. The majority of the data, and the data reported in this article, were obtained using the 3.18 mm nozzle. The test matrix is shown in table 1. All measurements were obtained with a measurement volume located 22 cm radially outward from the nozzle center line and in mid-stream between the top of the spray plume and the bottom. A series of tests were performed to locate this measurement position.

The measurement location was chosen to give a characteristic drop diameter distribution of the spray. A series of measurements were obtained at varying elevations and radii to characterize the influence of measurement volume position on the measured diameter distributions. It was determined that, (1), the drops are fully formed within approximately 10 cm radially outward of the breakup radius of the liquid fan sheet which flows from the plate and breaks into drops, and (2), at radial distances greater than approximately one half meter from the nozzle the smaller drops fall from the spray plume (due to higher frictional force with air per unit mass for small drops than large drops), and the diameter distribution becomes increasingly bimodal with distance (the bimodal nature of the distribution may be an indication of coalescence of drops in the spray according to Cadle (1965)). The spray was measured in the mid-plume elevation since the drop flux is largest there (permitting a high data acquisition rate), and because drop diameter distribution does not change significantly with vertical displacement in mid-plume. This is shown in figure 5. Outside the main spray plume diameter decreases with vertical distance from the plume, especially below the spray plume, where smaller drops settle out and form a visible low velocity cloud.

In addition to drop diameter distributions, the average radius of the liquid fan at breakup into drops was measured from photographs. The radius is uneven as may be seen in the photographs.

MEASUREMENT UNCERTAINTY

Assessment of PDPA measurement uncertainty is not straightforward. Although the instrument is calibrated by the manufacturer and the calibration was tested by measurements of monodisperse drop sizes produced by an Aerometrics monodisperse drop generator (the measurements agree to within a few percent of generated drop size), other errors may arise. Errors may be due to drops

Table 1. Test matrix. Delivery pressure (kPa gauge) at which data were obtained are given

Nozzle to plate distance (cm)	Plate diameter (cm)						
	0.89	1.27	1.90	2.54	3.18	3.81	5.08
0.10		69, 103,			138		
0.16		69, 103,			138		
0.32		138			138		
0.63		138			138		
1.27		138			138		
2.22	69, 103, 138	69, 103, 138, 172	103, 138	103, 138	69, 103, 138, 172	103, 138	103, 138
4.76	103, 138	69, 103, 138, 172	103, 138	103, 138	48, 69, 103, 138, 172	103, 138	103, 138
7.62		69, 103, 138, 172			69, 103, 138		
10.80	69, 103, 138			69, 103, 138			

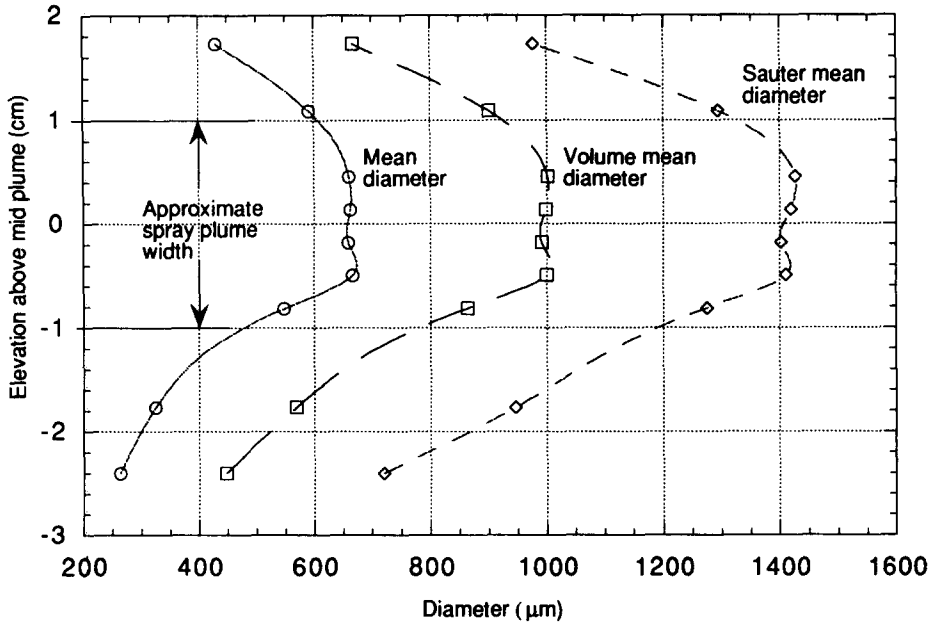

Figure 5. Drop diameter versus elevation (138 kPa gauge delivery pressure, 3.18 cm plate diameter, 2.22 cm nozzle to plate spacing).

with diameters smaller than the minimum for the measurement range, drops larger than the maximum for the measurement range, and non-spherical drops. The influence of drops with diameters less than the minimum measured size (typically 85.7 μm for these experiments) may be accounted for by repeating measurements using lower ranges. It was found that drop diameter number distributions continue to monotonically decrease with decreasing size. The influence of these small drops on diameter mean and especially on volume mean and Sauter mean is small (less than a few percent). Photographs show no drops larger than 3,000 μm for delivery pressures larger than approximately 60 kPa. Photographs also show that most, but not all, drops have become spherical before reaching the measurement volume. These few non-spherical drops are larger than approximately 2,000 μm. The maximum uncertainty due to non-spherical drops between 2,000 μm and 3,000 μm is estimated as the difference between diameter, volume, and Sauter means with the upper limits of two (or more) repeated measurements set at 2,000 μm and 3,000 μm for the same nozzle flow conditions.

These differences are considerably larger than the uncertainties attributed to other sources and are therefore taken as the estimated uncertainty of measurements.

Estimated uncertainties of diameter averages (for 10,000 samples)

diameter mean	+/− 60 μm
volume mean	+/−100 μm
Sauter mean	+/−100 μm,

other measurement uncertainties

pressure	+/−3 kPa
flow rate	+/−2%
temperature	+/−0.2°C
fan radius at breakup	+/−0.5 cm.

The uncertainty of fan sheet radius at breakup is due to the unevenness of breakup radius with angular position rather than measurement accuracy.

PHENOMENA OBSERVED

Photographs show the large-scale and small-scale phenomena associated with nozzle flow and liquid sheet and drop formation and flow. Five photographs are reproduced as figures 6–10.

Phenomena observed include the turbulence structure of the outside of the liquid jet, the flow of liquid across the plate, the liquid sheet, liquid sheet instabilities, and the breakup of the liquid sheet into drops.

The liquid jet emerging from the distribution nozzle exhibits structure as described by Hoyt & Taylor (1979), Mansour & Chigier (1994), and others. The jet propagates a distance from the nozzle equal to several nozzle diameters before a flat equilibrium velocity profile develops from a turbulent nozzle flow profile. For the Reynolds number range of interest ($>20{,}000$) the relaxation is completed within three jet diameters from the nozzle according to Mansour & Chigier (1994). Before equilibrium is established the jet displays a smooth surface, which may be seen in figure 7, although part of the region close to the nozzle is obscured in the photograph. Downstream of this region, the bumpy appearance of the turbulent jet, as shown in figures 6 and 7, is typical of the jet Reynolds number ($\mathrm{Re}_j = \rho_L U_j d_j / \mu$, where d_j is jet diameter, and μ is viscosity) range investigated (approximately 40,000–100,000). The jet does not disintegrate before impacting the plate, nor does it splatter upon impact.

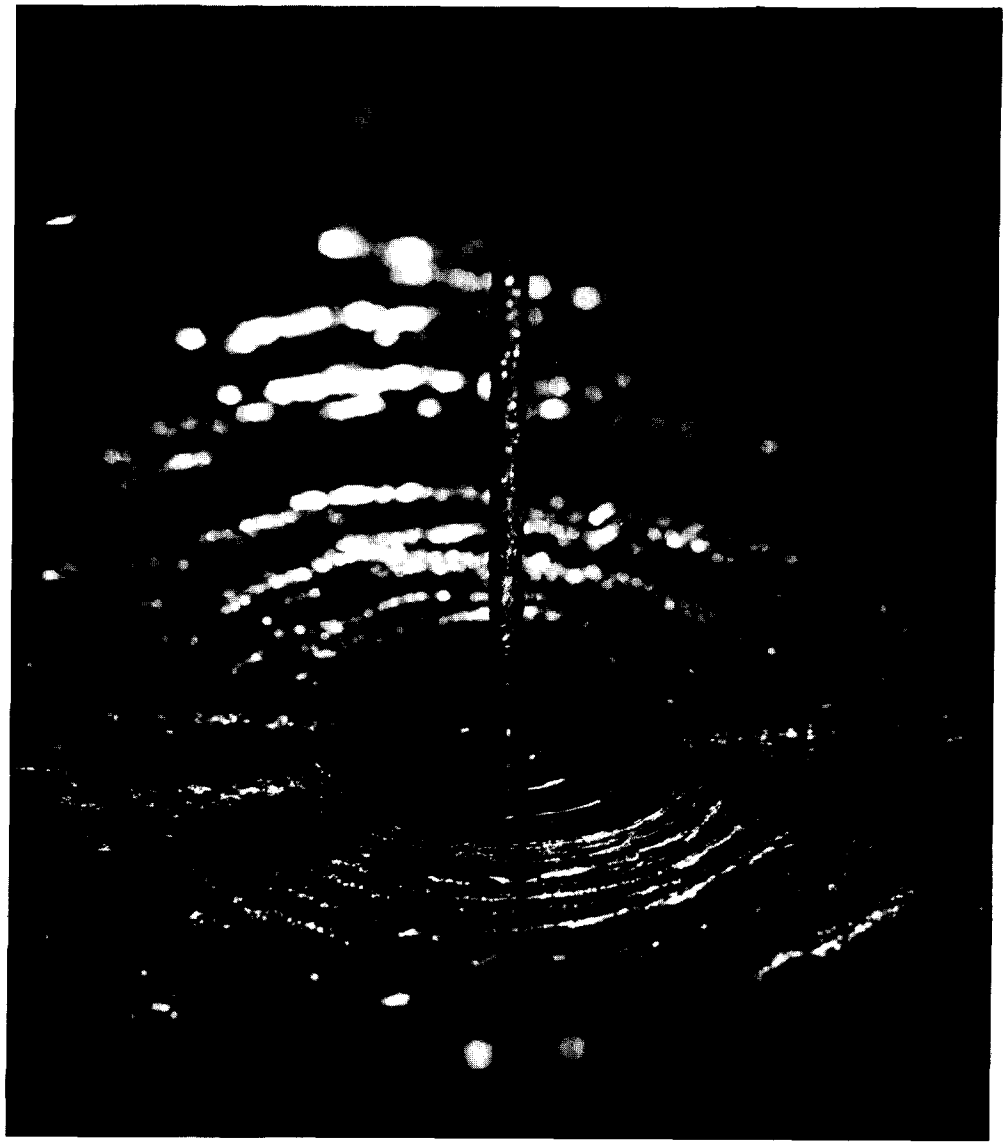

Figure 6. Liquid jet impacting flat plate (69 kPa gauge delivery pressure, 2.54 cm plate diameter, 1.87 cm nozzle to plate spacing).

After impact the jet spreads radially as a film. Stevens & Webb (1992) found that liquid surface velocity approached the mean jet velocity within a radial distance from the jet centerline of approximately 2.5 jet diameters (approximately 0.8 cm radius for our jet). Measured surface velocity continuously decreases radially outward from this position as the film thins due to radial expansion. Eventually, at radial distances greater than approximately seven jet diameters (approximately 2.2 cm radius for our jet), film thickness increases with radial distance as the boundary layer reaches the surface and shear forces slow the film flow.

Standing waves form on the liquid film attached to the plate with a wavelength approximately equal to jet diameter as may be seen in figure 6 (visually observing the flow with a stroboscope reveals that the average positions of the peaks of the waves remain stationary (standing), but oscillate somewhat erratically in time). The waves were observed by Bhunia & Lienhard V (1994a). Examining photographs of liquid film flow for various nozzle diameters ranging from 0.24 cm inside diameter to 1.27 cm inside diameter, and for various delivery pressures, revealed that the

Figure 7. Liquid jet impacting slightly concave plate (69 kPa gauge delivery pressure, 2.54 cm plate diameter, 1.87 cm nozzle to plate spacing, 1/18,000 s flash duration).

wavelength of the standing waves remains approximately equal to the jet diameter and does not noticeably vary with delivery pressure. This is in contrast with the waves on a liquid sheet produced by a colliding jet, where the wavelength decreases with the inverse of delivery pressure and is, to first order, not a function of jet diameter. It is interesting that measurements of average film thickness as a function of radius reported by Watson (1964), Olsson & Turkdogan (1966), Stevens & Webb (1992), Buyevich & Ustinov (1994), and others, do not capture these waves. This is probably due to the oscillations of the positions of the wave peaks. Time averaged measurements therefore show a flatter liquid surface than photographs reveal.

After the liquid sheet detaches from the plate the wavelength of standing waves approach that predicted by [1] before breakup, at least for lower delivery pressures. For the flow conditions shown

Figure 8. Liquid fan sheet breakup into drops (172 kPa gauge delivery pressure, 1.90 cm plate diameter, 1.87 cm nozzle to plate spacing).

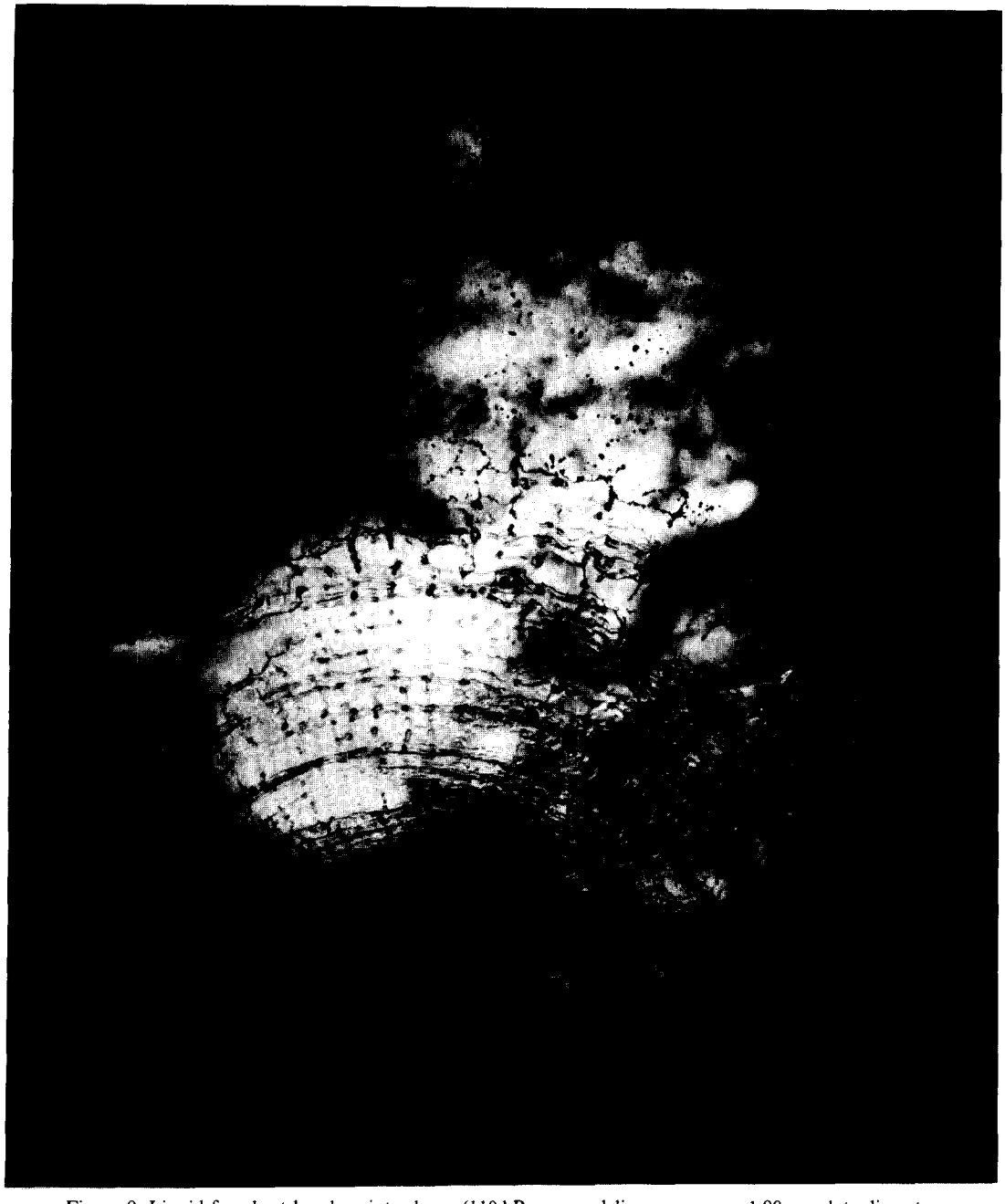

Figure 9. Liquid fan sheet breakup into drops (110 kPa gauge delivery pressure, 1.90 cm plate diameter, 1.87 cm nozzle to plate spacing).

in figure 6, the wavelength calculated by [1] is 0.64 cm, and the wavelength near the outer (in focus) radii shown in the photograph is approximately 0.6 cm. For higher delivery pressures, the breakup radius decreases, and the waves do not have sufficient time to relax to the wavelength limit for free sheets before breakup (this is discussed further in the next section).

The liquid sheet flows outward until it breaks into ligaments and then into drops, as may be seen in the photographs. Liquid sheet breakup into ligaments and then into drops is described by Dombrowski & Jones (1963). The authors describe the distance between ligaments as equal to the half wavelength of waves on the sheet. The existence of perforations in the sheet before breakup is consistent with the observations of Spielbauer & Aidun (1994).

Turbulent structures of the jet surface are seen to propagate outward on the liquid film surface as it flows across the plate and on the liquid sheet after it detaches from the plate. This is seen

Figure 10. Liquid fan sheet breakup into drops (69 kPa gauge delivery pressure, 1.90 cm plate diameter, 1.87 cm nozzle to plate spacing).

most clearly in figure 7. The photograph employed a slower flash duration (56 μs) and gives an indication of trajectories of the surface features by the streaks. The surface structure is progressively smoothed by surface tension forces, as may be seen by comparing figures 8–10. The turbulence surface structures reach the fan sheet radius at breakup into drops for the higher pressure case (172 kPa) shown in figure 8, but the surface is more smoothed for the intermediate pressure case (110 kPa) shown in figure 9 at the breakup radius, and smoother yet for the lower pressure case (69 kPa) shown in figure 10. Drop formation is therefore expected to be due to a combination of the surface tension and viscous force instability mechanisms proposed by Dombrowski & Jones (1963) and Spielbauer & Audin (1994), and the propagation of turbulent structures (both at the surface and internal to the flow) to the fan sheet breakup radius.

Splattering of the liquid jet, where drops are expelled from the liquid film upstream of the plate boundary, was not observed visually (using stroboscopic illumination). Splattering is governed by

the level of surface disturbances present on the surface of the jet according to Bhunia & Lienhard V (1994a). The jet surface was therefore sufficiently smooth to prevent splattering.

DROP DIAMETER DISTRIBUTIONS AND OTHER DATA

The drop diameter distribution data are presented as plots in this section to show the dependencies of size distributions on pressure, plate diameter, and nozzle to plate spacing. In addition to diameter distributions, the liquid fan radius at breakup into drops is discussed.

Delivery pressure upstream of the nozzle was used to set flow conditions in the experiments. Nozzle flow rate (Q) may be calculated as a function of delivery differential (gauge) pressure (P) and nozzle cross-section area (A_{noz}) as,

$$Q = C_d A_{noz} \sqrt{\frac{2g_c P}{\rho_L}}$$

where the experimentally determined discharge coefficient, $C_d = 0.95 \pm 0.02$, and g_c is the gravitational constant.

Several different size distributions have been used to characterize sprays. Drop diameter data is compared for one typical test with the commonly used log-normal distribution (Cadle 1965, Bolle & Moureau 1982), and the recently developed three parameter log-hyperbolic distribution (Durst *et al.* 1993) in figure 11.

The log-normal distribution, which is equivalent to a normal distribution of the logarithms of diameters is expressed as,

$$f(d) = \frac{1}{\xi d\sqrt{2\pi}} \exp\left(-\frac{1}{2}\left[\frac{\ln d/\bar{d}}{\xi}\right]^2 \right) \quad [2]$$

where d is drop diameter, $\bar{d}$ is the geometric mean diameter,

$$\bar{d} = \exp \sum_i \frac{n_i}{N} (\ln d_i) \quad [3]$$

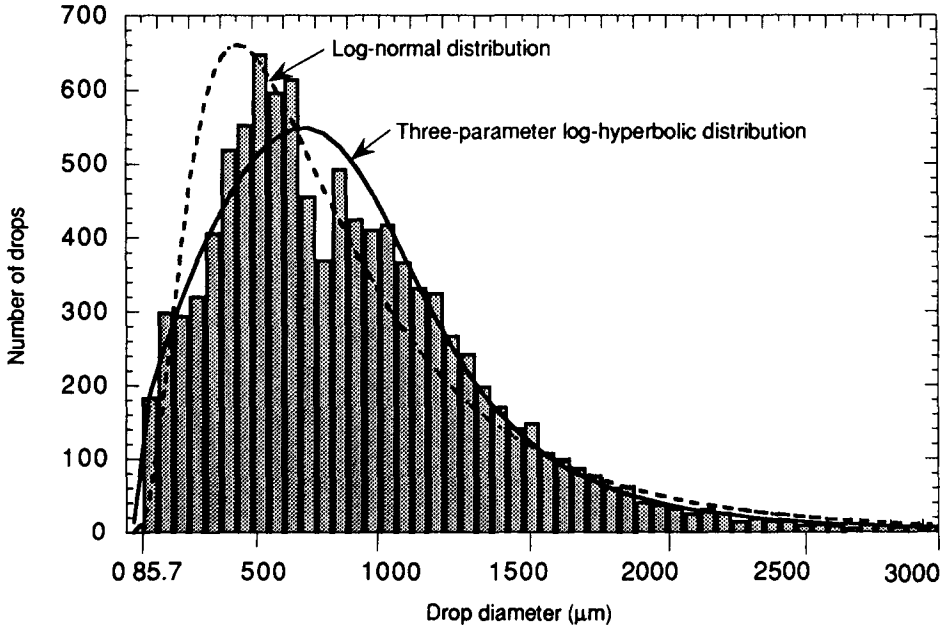

Figure 11. Comparison of data with log-normal and three-parameter log-hyperbolic distribution fits to data (138 kPa pressure, 5.18 cm plate diameter, 2.22 cm nozzle to plate spacing, 10,000 samples).

and the geometric standard deviation, ξ is defined by,

$$\xi^2 = \sum_i \frac{n_i}{N}\left[\ln\frac{d_i}{d}\right]^2, \quad [4]$$

where n_i is the number of drops in interval i with diameter d_i, and N is the total number of drops.

The three parameter log-hyperbolic distribution was developed from the observation that many particle size distributions are described by a hyperbola when drop diameter is plotted against the logarithm of the probability density function. Constants in the distribution relate to the position of the vertex of the hyperbola (v, v_0), the slopes of the included angle of the hyperbola (a), and the rotation of the axis of the hyperbola in the drop diameter versus the logarithm of the probability density function coordinates (θ). The probability density function $(h(d))$, termed the "three parameter hyperbolic distribution" is solved as (Durst *et al.* 1993),

$$h(d) = A\exp\left[-\frac{a}{a^2\cos^2\theta - \sin^2\theta}\sqrt{(a^2\cos^2\theta - \sin^2\theta) + (d + v_0 - v)^2}\right.$$
$$\left. - \frac{(a^2+1)\sin\theta\cos\theta}{a^2\cos^2\theta - \sin^2\theta}(d + v_0 - v)\right], \quad [5]$$

where

$$v_0 = -\frac{(a^2+1)\sin\theta\cos\theta}{\sqrt{a^2 - (a^2+1)^2(\sin^2\theta\cos^2\theta)/(a^2\cos^2\theta - \sin^2\theta)}} \quad [6]$$

and A is a normalization constant.

The distribution of $s = \exp(d)$ is then the three parameter log-hyperbolic distribution $(3P - H)$. Its probability density function is given by,

$$g(s) = \frac{1}{s}h(\ln s, a, \theta, v). \quad [7]$$

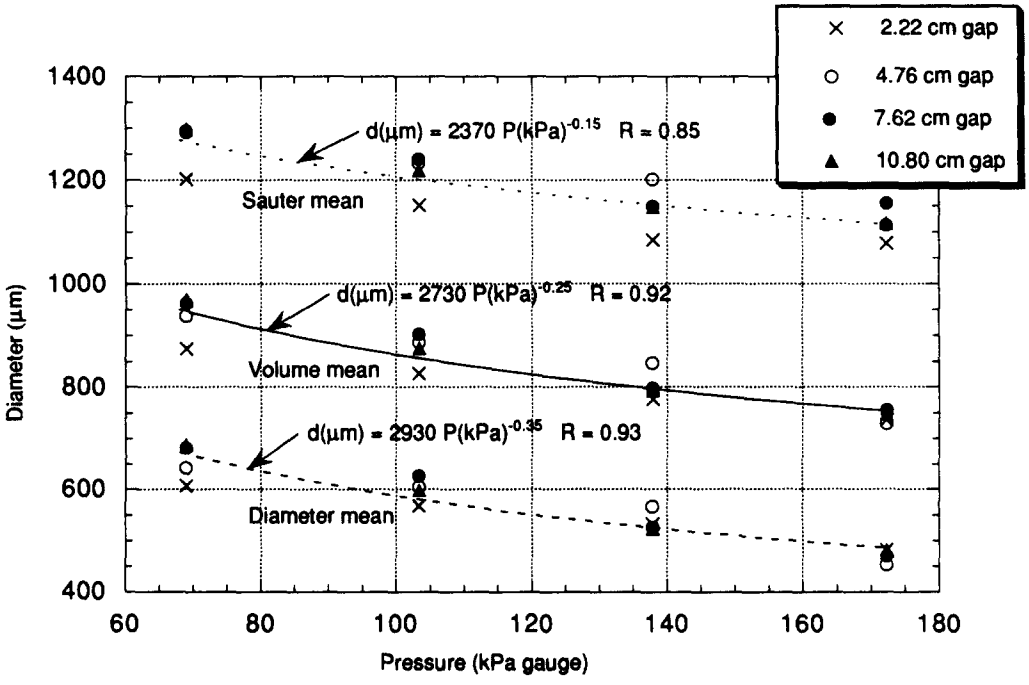

Figure 12. Drop diameter versus delivery pressure for 1.27 cm diameter plate, various nozzle to plate distances, and power law fits to data.

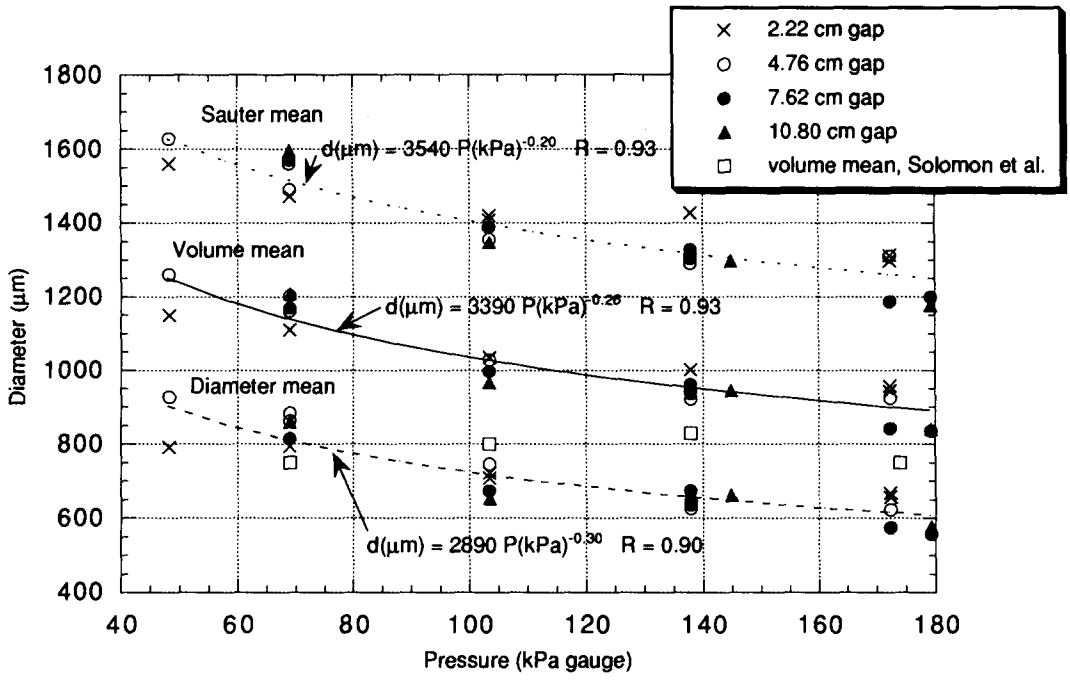

Figure 13. Drop diameter versus delivery pressure for 3.18 cm diameter plate, various nozzle to plate distances, and power law fits to data. Data of Solomon *et al.* (1966) shown.

The authors investigated several methods of estimating the three independent parameters (a, v, and θ) from data and found that a "maximum likeness estimation" is the best method.†

The comparison of the log-normal and the 3P-H distribution in figure 11 shows that, although either distribution gives a reasonable description of the middle region of the distribution, the 3P-H distribution better represents the data at small and large drop diameters. The better fit to the data is obtained at the expense of increased complexity (three independent parameters versus two).

Relevant averages related to a drop size distribution include the arithmetic mean diameter d_{10}, the volume mean diameter, d_{30}, and the Sauter mean diameter, d_{32}, which is the volume divided by area average. The ratios of data averages provide an indication of the standard deviation of the data. The larger the ratios the wider the distribution of drop diameters.

The data show that the drop diameter means decrease with increasing pressure. This is shown in figures 12 and 13. For the curve fits, P signifies pressure and R is the residual. Since jet velocity increases with the square root of pressure, and shear stress between the drop and air increases approximately with velocity squared, smaller drops form at higher jet velocities. The dependency is typically expressed by the non-dimensional Weber number (We), the ratio of dynamic pressure force divided by surface tension force (alternately defined by some authors as shear stress divided by surface tension force):

$$\mathrm{We} = \frac{\rho_G V^2 d}{\sigma},$$

where ρ_G is gas density, and V is drop velocity.

If maximum diameter drops form at constant critical maximum Weber number, and if diameter mean and volume mean diameters remain a constant fraction of maximum diameter over the pressure range of interest, then the diameter means should vary with the inverse of velocity squared, or equivalently, with the inverse of delivery pressure. For instance, Kocamustafaogullari *et al.* (1994) derive constant ratios of volume mean and Sauter mean diameters divided by maximum stable drop diameter which agree reasonably well with data for annular two-phase flow. The

†A computer program which solves the three parameter log hyperbolic distribution from input data may be obtained from one of its authors, Prof. C. Tropea, University of Erlangen–Nuremburg, 91058 Erlangen, Germany, e-mail: CTROPEA@LSTM.ERLANGEN.DE.

authors derive physically based correlations for the maximum and mean drop sizes in annular two-phase flow, and relate the maximum stable drop diameter to the turbulent kinetic energy dissipation rate and surface tension forces. The authors find that maximum stable drop size should vary with relative velocity to the $-14/15$ power. The experimental results of Jepson *et al.* (1989), show that the Sauter mean diameter of drops decreases approximately to the -1.2 power of relative velocity.

The data for spray nozzles show less dependency on velocity or delivery pressure than for entrained drops in annular flow. For cone type nozzles, the data of St Georges & Buchlin (1994) shows a variation of mean diameter proportional to delivery pressure to approximately the -0.37 power (or, with velocity to approximately the -0.61 power). Fraser *et al.* (1962) extended the theory of Squire (1953) to derive an expression for drop size produced by a low viscosity liquid sheet. Their expression for drop diameter (d) may be expressed as,

$$d \propto \left(\frac{\rho_L}{\rho_G}\right)^{1/6} \sigma^{1/3} P^{-1/3}, \qquad [8]$$

where P is nozzle delivery gauge pressure.

The dependency of drop diameter on pressure or jet velocity for our data, as is shown in figures 12 and 13, is considerably smaller than for annular flow, in approximate agreement with the theory of Fraser *et al.* (1962), and slightly smaller than the data reported above for cone type nozzles. Our data for a 1.27 cm diameter plate and various nozzle-to-plate distances shows a mean diameter dependency on pressure to approximately the 0.35 power and the data for a 3.18 cm diameter plate shows mean diameter varying to approximately the -0.30 power. Non-linear effects, such as the variation of liquid sheet and drop drag coefficients with liquid sheet and drop Reynolds numbers, and the influence of jet turbulence on drop formation, etc. probably affect the pressure dependency.

Drop diameter is also a function of distribution nozzle diameter, as discussed by Solomon *et al.* (1985). The reference reports that drop size increases with delivery nozzle inside diameter. However, any variation in drop diameter was less than measurement uncertainty for the two nozzle diameters investigated (2.29 and 3.18 mm i.d.).

The influence of nozzle-to-plate spacing on drop diameter is shown in figures 14 and 15. The most significant feature is the relatively small dependency of the diameter distributions on nozzle-to-plate spacing. The mean diameters vary by less than 30% over a two orders of magnitude range of nozzle to plate distance (0.10–10.8 cm). Since the distribution nozzle jet is not seen to expand significantly in the photographs, the jet velocity is approximately constant for the spacings

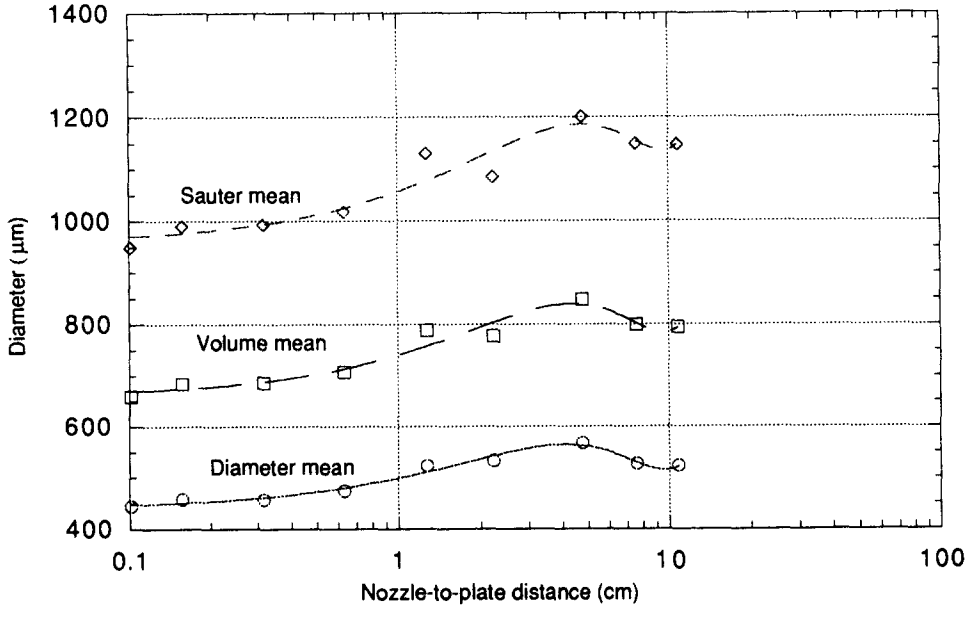

Figure 14. Drop diameter versus distribution nozzle to plate distance (138 kPa gauge pressure, 1.27 cm plate diameter) and third order polynomial fit to data.

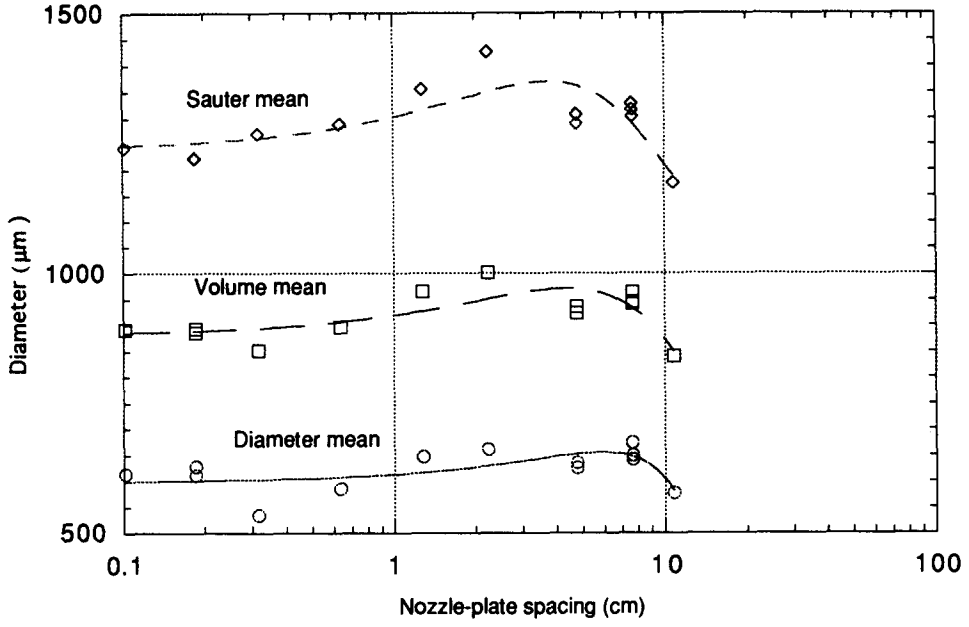

Figure 15. Drop diameter versus distribution nozzle to plate spacing (138 kPa gauge pressure, 3.18 cm plate diameter) and third order polynomial fit to data.

investigated. If it is assumed that the velocity of the liquid fan is approximately a constant fraction of jet velocity, then drop diameter should be approximately the same regardless of spacing. One perhaps surprising features of the data is that reducing the nozzle-to-plate distance to within one jet diameter, where the jet velocity profile has not yet reached equilibrium, does not significantly affect the drop diameter distribution.

The dependencies of drop diameter distribution on plate diameter, D, are shown in figures 16–19. Drop diameter increases monotonically with plate diameter for the lower pressure (103 kPa gauge) condition shown in figures 16 and 17. The diameter mean value was varied by more than a factor of 1.5 at this pressure by varying the plate diameter from 0.89 to 5.08 cm. The increase is not

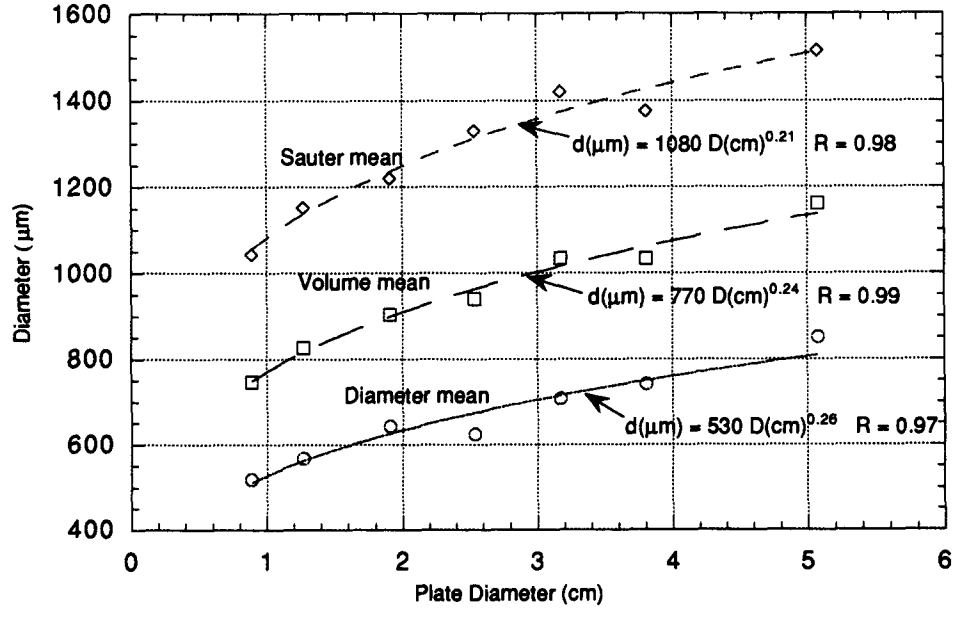

Figure 16. Drop diameter versus plate diameter (103 kPa gauge pressure, 2.22 cm nozzle to plate spacing) and power law fits to data.

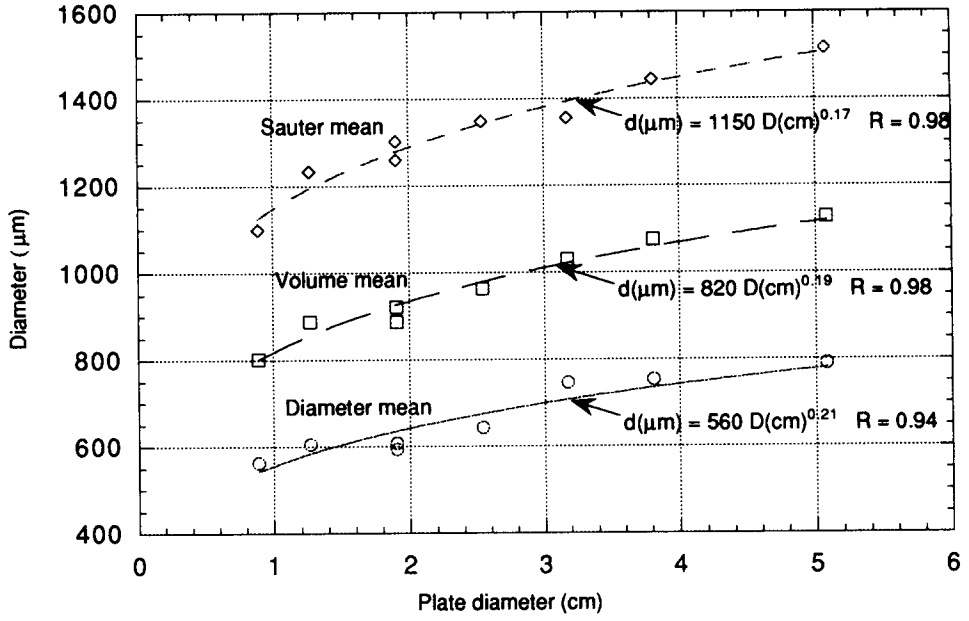

Figure 17. Drop diameter versus plate diameter (103 kPa gauge pressure, 4.76 cm nozzle to plate spacing) and power law fits to data.

monotonic for the higher pressure conditions shown in figures 18 and 19. A monotonic increase in drop diameter with plate diameter might be explained by lower liquid sheet velocity and increased sheet thickness caused by plate friction for larger plate diameters. An explanation for the non-monotonic dependency displayed in figures 18 and 19 is probably related to the shorter wavelength on the film attached to the plate which steadily increases to the wavelength given by [1] and the reduced breakup radius at higher pressure. If the wavelength at the similar breakup radius is shorter for larger plate diameters, then the resulting drop diameters should be smaller. Photographs reveal that the wavelength at breakup is indeed shorter for the larger diameter plate for the two higher pressures investigated (at still higher pressures, the wavelength at the breakup

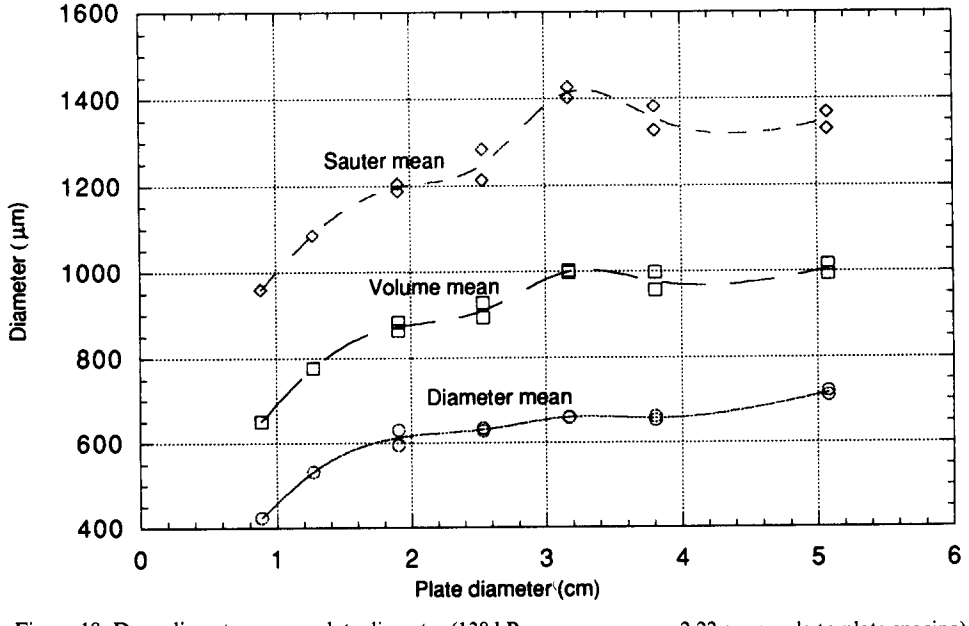

Figure 18. Drop diameter versus plate diameter (138 kPa gauge pressure, 2.22 cm nozzle to plate spacing) and cubic spline fit to data.

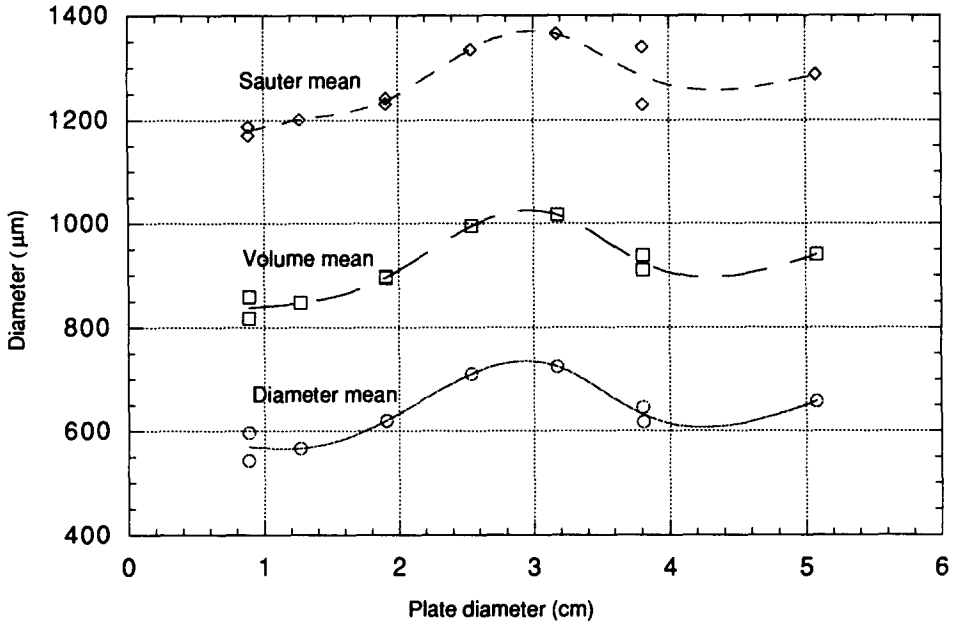

Figure 19. Drop diameter versus plate diameter (138 kPa gauge pressure, 4.76 cm nozzle to plate spacing) and cubic spline fit to data.

radius is approximately the wavelength on the plate, regardless of plate diameter). At the lower delivery pressures investigated, the wavelength at the larger breakup radius is approximately the same regardless of plate size. This is only a partial explanation, since the differences displayed in figure 18 compared to figure 19 depend on nozzle to plate spacing.

The dependency of drop diameter distribution on plate diameter at higher pressures should change with delivery nozzle size, since the wavelength of standing waves on the plate will change. However, this aspect was not investigated in the present study.

Only one known published study of drop size measurements for spray plate nozzles with similar distribution nozzle inside diameter as ours is available for direct comparison. The data are reported by Solomon *et al.* (1985). Four values of volume mean drop sizes for a distribution nozzle inside diameter of 3.18 mm are shown in figure 13. Measurements were obtained by capturing drops in pans of flour, and the diameters of the resulting pellets of water-flour measured. Water drop size was correlated to pellet size by calibration with known drop sizes. Drops were measured near the maximum radius of the spray and at ground level. The measurement location may account for the differences in measured diameters at lower pressures.

The ratios of d_{30}/d_{10} varied from approximately 1.25–1.50 for these experiments, and the ratios of d_{32}/d_{10} varied from approximately 0.65–0.72. In general, the ratios were closer to 1.0 at lower delivery pressures, which indicates that the standard deviation of drop sizes is smaller at lower delivery pressures. The influence of plate diameter and nozzle-to-plate spacing on the diameter mean ratios was smaller than the influence of pressure.

Although flat spray plates were primarily employed for our experiments, a few measurements were taken using a slightly concave plate (2.54 cm diameter, approximately 10 cm radius of curvature) were taken for comparison, since concave plates are used to modify the spray pattern. Drop diameter distribution was not affected by the concavity of the spray plate to within the uncertainty of measurement repeatability.

Spray fan radius at breakup, the radius of the liquid sheet at which drops form was measured from photographs. This is shown in figure 20. The measurements show no dependency (to within measurement uncertainty of ± 0.5 cm) of breakup radius on plate diameter. This is perhaps surprising since drop diameter is shown to vary with plate diameter. The data is compared with the semi-empirical equation of Huang (1970) for the breakup radius of a liquid sheet formed by colliding jets. Our measured breakup radius is smaller than for colliding jets. The primary reason may be due to the differing instability wavelengths (and amplitudes) produced by spray plates and

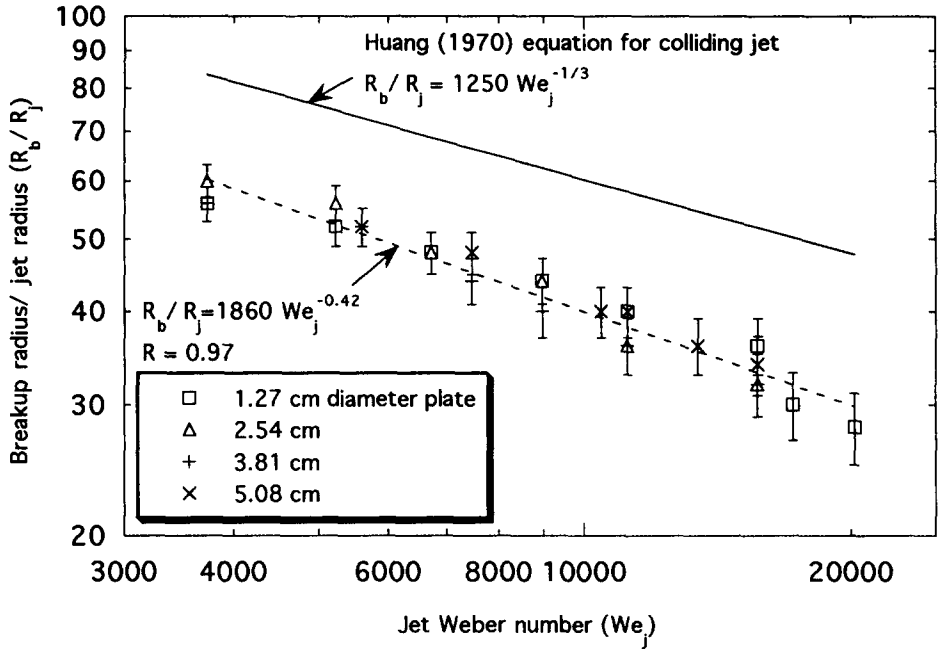

Figure 20. Non-dimensional breakup radius for various plate diameters, curve fit to data, and comparison with the semi-empirical equation for colliding jet breakup of Huang (1970).

colliding jets. The model of Huang (1970) predicts that the breakup radius should be approximately proportional to the product of sheet velocity times wavelength. Therefore, the effects of plate friction and decreased wavelength should both decrease breakup radius, although our data does not exhibit the simple velocity times wavelength product relationship of the model.

CONCLUDING REMARKS

Drop diameter distribution data for an adjustable spray plate nozzle were measured using a PDPA. Diameter mean, volume mean, and Sauter mean were calculated for each distribution. The three parameter log-hyperbolic distribution provided a closer fit to the data than did a log-normal distribution for the smallest and largest drops. Either distribution gives a reasonable representation of the middle region of the drop diameter distribution data.

Photographs show the large-scale and small-scale phenomena associated with nozzle flow and liquid sheet and drop formation and flow. Phenomena observed include the turbulence structure of the outside surface of the liquid jet, the flow of liquid across the plate, the free liquid sheet, liquid sheet instabilities, and the breakup of the liquid sheet into drops. Standing waves form on the liquid film attached to the plate with a wavelength approximately equal to jet diameter. Beyond the plate the wavelength progressively lengthens. The waves propagate outward to a radius of breakup into drops.

The experiments quantify the influence of plate diameter and nozzle-to-plate spacing on drop diameter distribution for spray plate nozzles. In general, drop diameter increases with plate diameter. The diameter mean value was varied by more than a factor of 1.5 in the experiments by varying the plate diameter. The dependence of drop diameter on plate diameter is monotonic at the lower delivery pressure investigated (103 kPa gauge), but is not monotonic at the higher delivery pressure investigated (138 kPa gauge). The dependence of drop diameter distribution on nozzle-to-plate spacing, is less dramatic than the dependence on plate diameter. The mean diameters vary by less than 30% over a two orders of magnitude range of nozzle to plate distance (0.1 cm to 10.8 cm).

Drop diameter decreases with increasing pressure, but to a much smaller power than predicted by a constant critical Weber number dependency. The pressure dependency on drop size is similar to, but slightly smaller than, that for cone type nozzles. The slopes of diameter versus pressure curves show only a small dependency on nozzle to plate spacing and on plate diameter.

Existing models of drop formation from nozzles, annular two-phase flow, or sheet flow help provide a physical explanation for the drop formation phenomena observed and the dependency of drop diameter on delivery pressure or sheet velocity. However, theoretical models that predict the dependencies of drop diameter distributions on plate diameter and nozzle-to-plate spacing are still lacking.

The results of these and future experiments should be useful to spray nozzle designers since design parameters can be varied to provide desired drop diameter distributions within a limited range.

Acknowledgements—This research was sponsored by the Lockheed Idaho Technologies Company Laboratory Directed Research and Development Program and Experimental Thermal Science Long Term Research Initiative. The authors gratefully acknowledge help from Dr Dennis Kincaid of the USDA Agriculture Research Service, Kimberly, Idaho, Dr David Zoldoske of the Center for Irrigation Technology, Fresno, California, John Capek of Lockheed Idaho Technologies Company who did the large format photography and darkroom work, and Dennis Phetteplace who built much of the experiment apparatus. Professor Cameron Tropea of the University of Erlangen, Germany, graciously provided the computer program to calculate the three parameter log–hyperbolic distribution.

REFERENCES

Bachalo, W. D., Rudoff, R. C. & Sankar, S. V. 1990 Time resolved measurements of spray drop size and velocity. In *Liquid Particle Measurement Techniques* (Edited by Hirleman, E. D., Bachalo, W. D. & Felton, P. G.), ASTM STP 1083 pp. 209–224. American Society of Testing and Materials, Philadelphia.

Bhunia, S. K. & Lienhard, V. J. H. 1994 Splattering during turbulent liquid jet impingement on solid targets. *ASME J. Fluids Engineering* **116,** 338–344.

Bhunia, S. K. & Lienhard, V. J. H. 1994 Surface disturbance evolution and the splattering of turbulent liquid jets. *AMSE J. Fluids Engineering* **116,** 721–727.

Bolle, L. & Moureau, J. C. 1982 Spray cooling of hot surfaces. In *Multiphase Science and Technology* (Edited by Hewitt, G. F., Delhaye, J. M. & Zuber, N.), Vol. 2. Hemisphere Publishing, New York.

Buyevich, Y. A. & Ustinov, V. A. 1994 Hydrodynamic condition of transfer processes through a radial jet spreading over a flat surface. *Int. J. Heat Mass Transfer* **37,** 165–173.

Cadle, R. D. 1965 *Particle Size, Theory and Industrial Applications.* Reinhold, New York.

Chin, L. P., Larose, P. G., Tankin, R. S., Jackson, T., Stutrud, J. & Switzer, G. 1991 Droplet distributions from the breakup of a cylindrical liquid jet. *Phys. Fluids A* **3,** 1897–1906.

Clift, R., Grace, J. R. & Weber, M. E. 1978 *Bubbles, Drops and Particles.* Academic Press, New York.

Dombrowski, N. & Johns, W. R. 1993 The aerodynamic instability and disintegration of viscous liquid sheets. *Chem. Engr. Sci.* **18,** 203–214.

Durst, F., Tropea, C. & Xu, T. H. 1993 The three parameters log–hyperbolic distribution and its application to droplet size distributions. *Atomization and Sprays* **3,** 103–124.

Elison, B. & Webb, B. W. 1994 Local heat transfer to impinging liquid jets in the initially laminar, transitional, and turbulent regimes. *Int. J. Heat Mass Transfer* **37,** 1207–1216.

Fraser, R. P., Eisenklam, P., Dombrowski, N. & Hasson, D. 1963 Drop formation from rapidly moving sheets. *AIChE J.* **8,** 672–680.

Hawkes, R. D., Martin, D. L. & Meyer, G. 1992 In flight behavior of sprinkler drops by digital image analysis. ASAE paper 92-2526, American Society of Agricultural Engineers, St. Joseph, MI.

Hoyt, J. W. & Taylor, J. J. 1979 Effect of nozzle shape and polymer additives on water jet appearance. *J. Fluids Engineering* **101,** 304–308.

Jepson, D. M., Azzopardi, B. J. & Whalley, P. B. 1989 The effects of gas properties on drops in annular flow. *Int. J. Multiphase Flow* **15,** 327–339.

Kincaid, D. C. 1993 Sprinkler droplet kinetic energy and erosion potential, ASAE paper 932102, American Society of Agricultural Engineers, St. Joseph, MI.

Kincaid, D. C. & Longley, T. S. 1989 A water droplet evaporation and temperature model. *Trans. ASAE* **32,** 457–463.

Kocamustafaogullari, G., Smits, S. R. & Razi, J. 1994 Maximum and mean droplet sizes in annular two-phase flow. *Int. J. Multiphase Flow* **37,** 955–965.

Kolev, N. I. 1993 Fragmentation and coalescence dynamics in multiphase flows. *Experimental Thermal and Fluid Science* **6,** 211–251.

Lefebvre, A. H. 1989 *Atomization and Sprays.* Hemisphere, Washington DC.

Liu, X., Gabor, L. A. & Lienhard, V. J. H. 1993 Stagnation-point heat transfer during impingement of laminar liquid jets: analysis including surface tension. *ASME J. Heat Transfer* **115,** 99–105.

Mansour, A. & Chigier, N. 1994 Turbulence characteristics in cylindrical liquid jets. *Phys. Fluids* **6,** 3380–3391.

Olsson, R. G. & Turkogan, E. T. 1966 Radial spreading of a liquid stream on a horizontal plate. *Nature* **211,** 813–816.

Rayleigh, Lord 1878 On the instability of jets. *Proc. London Math. Soc.* **10,** 4–13.

Solomon, K. H., Kincaid, D. C. & Bezdek, J. C. 1985 Drop size distributions for irrigation spray nozzles. *Trans. ASAE* **28,** 1966–1974.

Solomon, K. H., Zoldoske, D. F. & Oliphant, J. C. 1991 Laser optical measurement of sprinkler drop sizes. *Proc. 1991 ASAE Winter Meeting*, Chicago, pp. 87–96.

Spielbauer, T. M. & Aidun, C. K. 1994 The wave thinning and breakup of liquid sheets. *AMSE J. of Fluids Engineering* **116,** 728–734.

Squire, H. B. 1953 Investigation of the instability of a moving liquid film. *Brit. J. App. Physics* **4,** 167–169.

Stevens, J. & Webb, B. W. 1992 Measurements of the free surface flow structure under an impinging, free liquid jet. *J. Heat Transfer* **114,** 79–84.

St Georges, M. & Buchlin, J. M. 1994 Detailed single spray experimental measurements and one-dimensional modelling. *Int. J. Multiphase Flow* **20,** 979–992.

van der Geld, C. W. M. & Vermeer, H. 1994 Prediction of drop size distributions in sprays using the maximum entropy formalism: the effect of satellite formation. *Int. J. Multiphase Flow* **20,** 363–381.

Watson, E. J. 1964 The radial spreading of a liquid jet over a horizontal plane. *ASME J. Fluid Mechanics* **20,** 481–499.

Yarin, A. L. 1993 *Free Liquid Jets and Films: Hydrodynamics and Rheology.* John Wiley, New York.